AIP Conf. Proc. 963, 533 (2007)

Proceedings of ICCMSE 2007
(International Conference in Computational Methods in Science and Engineering 2007)

Controlled Intersubband Population Dynamics in a Semiconductor Quantum Well

Emmanuel Paspalakis[*], Constantinos Simserides[*] and Andreas F. Terzis[†]

[*]*Materials Science Department, School of Natural Sciences, University of Patras, Patras 265 04, Greece*
[†]*Physics Department, School of Natural Sciences, University of Patras, Patras 265 04, Greece*

Abstract. We examine the intersubband transition dynamics of a single semiconductor quantum well when the ground and the first excited subbands are coupled by strong electromagnetic fields, with emphasis given to controlled intersubband population inversion. The system dynamics is described by the nonlinear density matrix equations that include the effects of electron-electron interactions. We present analytical results for the electromagnetic field that can lead to high-efficiency population inversion in the system. The validity of the analytical results is tested with numerical solutions of the density matrix equations for various values of the electron sheet density for a realistic GaAs/AlGaAs quantum well.

Keywords: Coherent control, population transfer, inversion, semiconductor quantum well, intersubband transitions, two-subband system, pulsed electromagnetic field, density matrix equations
PACS: 78.67.De, 42.50.Hz, 73.21.Fg, 03.67.Lx

INTRODUCTION

In recent years the interaction of intersubband transitions of semiconductor quantum wells with strong electromagnetic fields is a topic of increasing interest due to the several potential applications of these structures. Several experiments in the past decade have revealed that quantum coherence and interference effects, such as tunneling induced transparency [1, 2], electromagnetically induced transparency [3], Rabi oscillations [4], pulsed-induced quantum interference [5], Autler-Townes splitting [6], and gain without inversion [7] can occur in intersubband transitions of semiconductor quantum wells. These experimental results have been explained quantitatively by atomic-like, non-interacting, multi-level systems interacting with external electromagnetic fields without accounting for the effects of electron-electron interactions.

In a quantum well the many-body effects arising due to the macroscopic carrier density play a significant role and make the system behaving quite differently than a non-interacting atomic-like system. Many-body effects have been studied in several theoretical works [8, 9, 10, 11, 12, 13, 14, 15, 16, 17, 18, 19, 20, 21, 22, 23, 24, 25] and in some experimental studies [26, 27, 28, 29, 30], where it has been shown that the optical response and the electron dynamics of the quantum wells can be significantly influenced by varying the macroscopic carrier density.

An important problem in this area is the potential for controlled population transfer and Rabi oscillations between two subbands in a semiconductor quantum well structure [21, 22, 23, 24, 25]. This problem was first studied by Batista and Citrin [21] including the many-body effects arising from the macroscopic carrier density of the system. For the dynamics of the system they used the density matrix equations obtained from a time-dependent Hartree approach [16]. They showed that the inclusion of the electron-electron interactions makes the system behaving quite differently from an atomic-like two-level system. To succeed high-efficiency population inversion and Rabi oscillations in a two-subband *n*-type modulation-doped semiconductor quantum well they used the interaction with a specific pulsed electromagnetic field with time-dependent frequency (chirped electromagnetic field). Their method was refined in a following publication where only linearly chirped pulses were used for high-efficiency intersubband population inversion [25] and was also applied to three-subband quantum well systems [22].

Different approaches for creating high-efficiency intersubband population inversion were proposed by two of us [23, 24]. In these studies the effective nonlinear Bloch equations of Olaya-Castro *et al.* [18] were used for the description of the system dynamics. Using analytical solutions of these equations, under the rotating wave approximation (RWA), we presented closed form analytical solutions for the electric field amplitude of the electromagnetic field that leads to high-efficiency population inversion. The validity of these solutions were accessed for a realistic double GaAs/AlGaAs quantum well structure.

In this article we continue our work on controlled population dynamics and creation of high-efficiency intersubband

population inversion in a semiconductor quantum well. Here, the dynamics of the quantum well system under the interaction with an electromagnetic field is described by the nonlinear density matrix equations of Galdrikian and Birnir [11]. These equations have been used successfully for the description of experiments on the optical properties of *n*-doped quantum wells [26, 27, 28]. We first apply the RWA and simplify the nonlinear density matrix equations. With the use of analytical solutions of these simplified density matrix equations we present closed form solutions for the electric field envelope of the applied electromagnetic field that leads to complete population inversion in the system, in the absence of any relaxation processes. For a realistic single GaAs/AlGaAs quantum well, in the presence of decay and dephasing processes, we show that high-efficiency population inversion is possible for specific values of the electron sheet density. We also explore the dependence of the analytical solutions and of the efficiency of the population inversion to the electron sheet density.

NONLINEAR DENSITY MATRIX EQUATIONS

We consider a single quantum well GaAs/AlGaAs. It is assumed that only the lower two energy subbands, $n = 0$ for the lowest subband and $n = 1$ for the excited subband, contribute to the system dynamics. The Fermi level is below the second subband minimum, so the excited subband is initially empty. This is succeeded by a proper choice of the electron sheet density. The quantum well interacts with an electromagnetic field with time-dependent electric field $E(t) = \mathscr{E}_0(t)\cos[\omega t + \phi(t)]$, where $\mathscr{E}_0(t)$ is the time-dependent electric field envelope, ω is the angular frequency and $\phi(t)$ the time-dependent frequency of the applied electric field. As it has been shown by Galdrikian and Birnir [11] (see also [15]) the system dynamics can be described by the following nonlinear density matrix equations:

$$\dot{\Delta}(t) = -\Gamma_1[\Delta(t) - \Delta_0] + \frac{4ez_{10}E(t)}{\hbar}\mathrm{Im}[\rho_{10}(t)] + 4\alpha\mathrm{Re}[\rho_{10}(t)]\mathrm{Im}[\rho_{10}(t)]\,, \tag{1}$$

$$\dot{\rho}_{10}(t) = -(\Gamma_2 + i\omega_{10})\rho_{10}(t) - i\frac{ez_{10}E(t)}{\hbar}\Delta(t) - i\alpha\mathrm{Re}[\rho_{10}(t)]\Delta(t)\,. \tag{2}$$

Here, $\Delta(t) = \rho_{00}(t) - \rho_{11}(t)$ $[\Delta_0 = \Delta(t=0)]$, with $\rho_{nm}(t)$ being the density matrix elements. Also, $\omega_{10} = (E_1 - E_0)/\hbar$ is the energy difference, where E_0, E_1 are the eigenvalues of energy for the ground and excited states in the well. In addition, $z_{10} = \int_{-\infty}^{\infty} dz\xi_1^*(z)z\xi_0(z)$ is the electric dipole matrix element between the two subbands, where $\xi_i(z)$, is the envelope function for the *i*-th subband along the growth direction (*z*-axis). Finally, α is the depolarization shift term [11, 15] that occurs due to the electron-electron interactions, and it is given by

$$\alpha = -\frac{8\pi e^2 N}{\hbar\varepsilon}\int_{-\infty}^{\infty} dz\xi_1^*(z)\xi_0(z)\int_{-\infty}^{z} dz'\int_{-\infty}^{z'} dz''\xi_1^*(z'')\xi_0(z'')\,. \tag{3}$$

Here, N is the electron sheet density, ε is the relative dielectric constant and e is the electron charge. Finally, in Eqs. (1) and (2) the terms containing the population decay rate Γ_1 and the dephasing rate Γ_2 describe relaxation processes in the quantum well and have been added phenomenologically in the nonlinear density matrix equations.

We note that we have taken the two subbands to have the same effective mass. As a result of this reason, in addition to the phenomenological approach of decay, the **k**-th dependence of the above parameters have been suppressed, where **k** is the wave-vector in the $x-y$ plane. We stress that the above approximations to the interaction of the electromagnetic fields with the quantum well structure, as well as the phenomenological approach of treating the decay mechanisms, have been proven well-suited to modeling quantitatively several experimental results [26, 27, 28].

We will now proceed with the RWA. We introduce the variable $\sigma_{10}(t) = \rho_{10}(t)\exp[i\omega t + i\phi(t)]$. If we ignore terms containing $\exp(\pm 2i\omega t)$ then, equations (1) and (2) reduce to

$$\dot{\Delta}(t) = -\Gamma_1[\Delta(t) - \Delta_0] - 2\Omega_0(t)\mathrm{Im}[\sigma_{10}(t)]\,, \tag{4}$$

$$\dot{\sigma}_{10}(t) = -\Gamma_2\sigma_{10}(t) - i[\omega_{10} - \omega - \dot{\phi}(t)]\sigma_{10}(t) + i\frac{\Omega_0(t)}{2}\Delta(t) - i\frac{\alpha}{2}\sigma_{10}(t)\Delta(t)\,, \tag{5}$$

where the time-dependent Rabi frequency is given by $\Omega_0(t) = -ez_{10}\mathscr{E}_0(t)/\hbar$.

ANALYTICAL SOLUTIONS

In order to obtain analytical solutions of Eqs. (4) and (5) we assume that there are no relaxation processes in the system, i.e. that $\Gamma_1 = \Gamma_2 = 0$. In addition, in our calculations we take the system initially in the lowest subband. Then,

the initial conditions are $\Delta_0 = 1$ and $\rho_{10}(t=0) = \sigma_{10}(t=0) = 0$. We now derive analytical solutions for the nonlinear density matrix equations under the RWA, Eqs. (4) and (5), for three specific cases:

First Case: Continuous Wave Field at Exact Resonance

For the first case we study the two-subband system excited by a continuous wave (CW) electromagnetic field, i.e. $\mathscr{E}_0(t) = \mathscr{E}_0$, at exact resonance with the corresponding quantum well transition, i.e. with $\omega = \omega_{10}$. In this case, starting from Eqs. (4) and (5) and following the same methodology as in Ref. [24] we obtain

$$\Delta(t) = \mathrm{cn}\left(\Omega_0 t | k = \frac{\alpha^2}{16\Omega_0^2}\right), \tag{6}$$

where cn is an elliptic Jacobi function and k is the parameter of cn. According to the above analytical result if $\Omega_0 > \alpha/4$ the system oscillates between the two subbands and complete transfer of electrons to the upper subband can occur. However, if $\Omega_0 < \alpha/4$ the electrons still oscillate between the two subbands, without complete inversion, with more population on average in the lower subband. Finally, if $\Omega_0 = \alpha/4$, $\Delta(t) = \mathrm{sech}(\Omega_0 t)$, so after an initial transient period the electron population is equally distributed in the two subbands. We also note that in the case that $\Omega_0 \gg \alpha/4$, then $\Delta(t)$ is approximated by $\Delta(t) \approx \cos(\Omega_0 t)$, that is the value of $\Delta(t)$ in the absence of electron-electron interactions.

The period of the above mentioned oscillations is given by

$$T = \frac{8}{\alpha}\int_0^{\pi/2} d\theta \left[1 - \frac{16\Omega_0^2}{\alpha^2}\sin^2\theta\right]^{-1/2}, \qquad \text{if} \qquad \Omega_0 < \alpha/4, \tag{7}$$

and

$$T = \frac{4}{\Omega_0}\int_0^{\pi/2} d\theta \left[1 - \frac{\alpha^2}{16\Omega_0^2}\sin^2\theta\right]^{-1/2}, \qquad \text{if} \qquad \Omega_0 > \alpha/4\,. \tag{8}$$

In cases that $\Omega_0 \gg \alpha/4$ the period of Rabi oscillations is approximated by the atomic Rabi oscillation period result, $T \approx 2\pi/\Omega_0$. If Ω_0 approximates $\alpha/4$ then, in the region $\Omega_0 > \alpha/4$, the oscillation period increases with decrease of Ω_0. Also, the shape of oscillations changes from sinusoidal to a more complex shape. In the region $\Omega_0 < \alpha/4$ the oscillation period decreases with decrease of Ω_0 and at the same time the average population in the lower subband increases.

Second Case: Hyperbolic Secant Pulse

For the second case we study the two-subband system excited at resonance $(\omega = \omega_{10})$ by a hyperbolic secant form electromagnetic pulse without chirping ($\phi(t) = 0$). In this case, $\Omega_0(t) = \bar{\Omega}\mathrm{sech}[(t-t_0)/t_p]$. Here, t_0 is the center of the pulse and it is chosen such that the electric pulse is practically zero at $t = 0$ (and $t = 2t_0$), t_p is the width of the pulse and $\bar{\Omega}$ is the maximum of the Rabi frequency. In the case that $\bar{\Omega}$ is chosen such that

$$\bar{\Omega} = \sqrt{\frac{\alpha^2}{4} + \frac{1}{t_p^2}}, \tag{9}$$

the analytic solution of equations (4)-(5) is given by

$$\Delta(t) = -\tanh\left(\frac{t-t_0}{t_p}\right). \tag{10}$$

Therefore, at $t = 2t_0$, $\Delta(t) \to -1$ and all the electrons are transferred in the upper subband. So, there is complete inversion in the system.

Third Case: Chirped Hyperbolic Secant Pulse

For this last case we consider the two-subband system excited by a chirped hyperbolic secant electromagnetic field. At $t = 0$ the central frequency of the field ω is chosen such that $\omega = \omega_{10}$. In this case, too, the time-dependent Rabi frequency is $\Omega_0(t) = \bar{\Omega}\text{sech}[(t-t_0)/t_p]$. If now

$$\dot{\phi}(t) = -\frac{\alpha}{2}\tanh[\frac{t-t_0}{t_p}] \quad \text{and} \quad \bar{\Omega} = \frac{1}{t_p}\,, \tag{11}$$

then from equations (4)-(5) we obtain

$$\Delta(t) = -\tanh\left(\frac{t-t_0}{t_p}\right). \tag{12}$$

Therefore, in this case, too, we obtain complete population inversion in the system at $t = 2t_0$.

QUANTUM WELL STRUCTURE CALCULATIONS

As we have mentioned above we consider a single GaAs/AlGaAs quantum well structure. Specifically, a GaAs layer is sandwiched between $Al_xGa_{1-x}As$ layers of sufficient width so that at both ends flat-band conditions prevail. The band offset used is 200 meV, roughly corresponding to Al mole fraction, x = 0.2. A 10 nm $Al_xGa_{1-x}As$ spacer is used on each side of the GaAs quantum well, followed by homogeneously donor-doped and ultimately by undoped $Al_xGa_{1-x}As$ layers. A slight unintentional acceptor doping, approximately three orders of magnitude smaller than the donor doping is assumed everywhere. We suppose that the samples have been illuminated and hence all donors are ionized. The charge neutrality condition provides the correct value of the chemical potential which is identified with the "zero energy". The temperature is taken $T = 4.2$ K. We notice that "spatial confinement" is not synonymous here to the "well width". In other words, increase of the doping level provides more electrons to the quantum well, and therefore another important factor must be taken into account: the redistribution of carriers which results in a "soft" barrier between the two AlGaAs/GaAs heterojunctions, in contrast to the double square quantum wells with the well known "hard" barrier. We discuss results corresponding to quantum well width of 30 nm.

Within the envelope function approach and the effective mass approximation, supposing for simplicity that the effective mass is constant everywhere, we solve self-consistently and numerically the effective mass equation

$$[-\frac{\hbar^2}{2m^*}\frac{d^2}{dz^2} + U(z) - E_i]\xi_i(z) = 0, \tag{13}$$

where $\xi_i(z)$ are the subband envelope functions and E_i the corresponding eigenenergies, and the so-called "Poisson" equation, i.e. the Gauss law

$$\nabla \cdot \mathrm{D} = \rho, \tag{14}$$

where ρ is the charge density. This way we obtain the electron subband structure and the sheet electron concentration using the structural and material details presented above. We note that we do not make any arbitrary assumptions for the number of the existing subbands and the form of the envelope functions. The conduction-band electron potential energy is [31]

$$U(z) = U_c(z) + U_{band\ offset} + U_{xc}(z). \tag{15}$$

Here, $U_{band\ offset}$ is the potential energy term due to the discontinuities of the conduction band minimum i.e. because of the different materials, $U_c(z)$ is the Coulombic potential energy obtained by the solution of Eq. 14, and $U_{xc}(z)$ is the exchange and correlation potential energy. For U_{xc} we use the expression of Hurkx and van Haeringen [32] which is the dominant term in the full expression given by Stern and Das Sarma [33]. The algorithm used to solve self-consistently Eqs. (13)-(15) has been described in Ref. [31], as well as an algorithm which may be used when non-parabolicities are important can be found elsewhere [34].

We note that we have performed structure calculations with both homogeneous doping (as described above) and with Si δ-type doped layers put symmetrically far away from the quantum well. In addition, we have performed calculations without accounting for the exchange and correlation potential energy term (U_{xc}) in the conduction band potential energy, as was proposed in the original paper of Galdrikian and Birnir [11] (see also [15]) for both homogeneous

TABLE 1. Calculated parameters for the quantum well structure under study for several electron sheet densities.

$N(\times 10^{11}$ **cm**$^{-2})$	$E_1 - E_0$ **(meV)**	z_{10} **(nm)**	$\hbar\alpha$ **(meV)**
0.4	14.85	-6.07	2.09
0.7	14.47	-6.13	3.72
1	14.08	-6.20	5.41
2	12.82	-6.45	11.45
3	11.60	-6.70	18.20
4	10.63	-6.93	25.51

and Si δ-type doping. For the quantum well structure and the electron sheet densities under study all the above calculations gave quite similar results for the energies, the matrix elements and the depolarization shift. The results of our calculations for several electron sheet densities are given in Table 1.

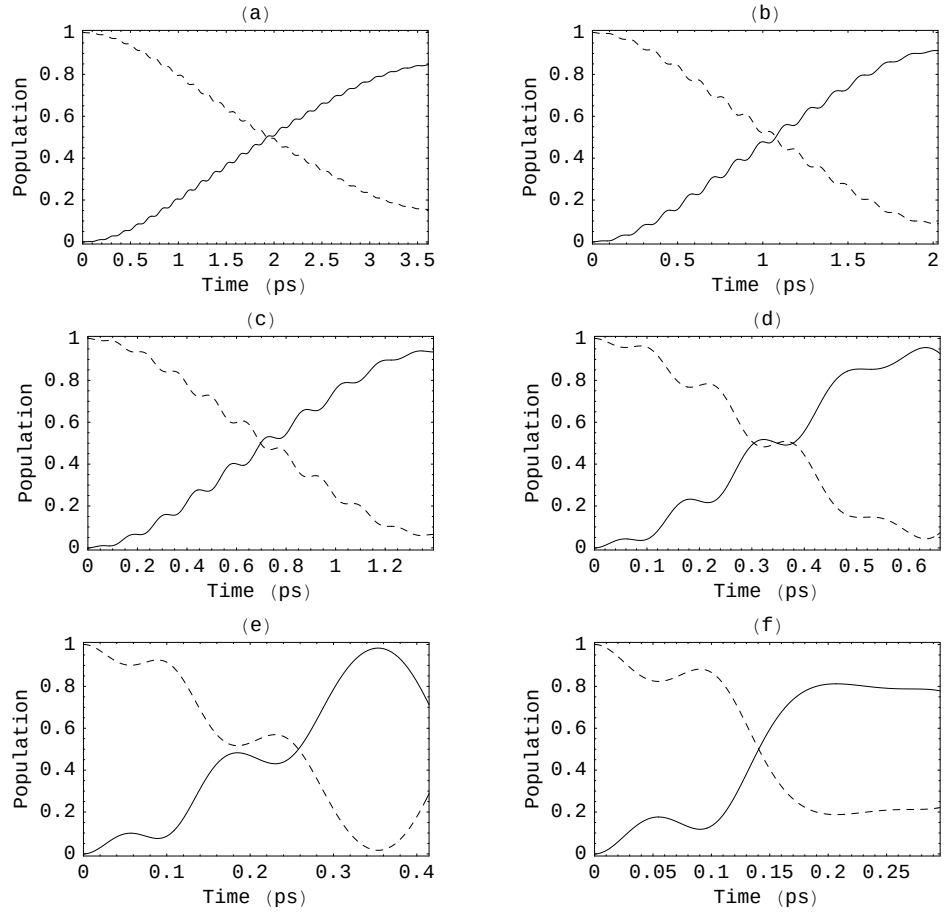

FIGURE 1. The time evolution of the population in the two subbands, lower subband (dashed curve) and upper subband (solid curve), obtained from numerical solution of the nonlinear density matrix equations (1) and (2) for a CW electromagnetic field. In these calculations $\Omega_0 = \alpha/3$ and $\omega = \omega_{10}$. In (a) $N = 4\times 10^{10}$ cm^{-2}, (b) $N = 7\times 10^{10}$ cm^{-2}, (c) $N = 1\times 10^{11}$ cm^{-2}, (d) $N = 2\times 10^{11}$ cm^{-2}, (e) $N = 3\times 10^{11}$ cm^{-2}, and (f) $N = 4\times 10^{11}$ cm^{-2}.

NUMERICAL RESULTS FOR THE TIME EVOLUTION OF POPULATIONS

We will assess the validity of the analytical results for creating high-efficiency intersubband population inversion using numerical solutions of the nonlinear density matrix equations (1) and (2). As we are interesting in describing a realistic quantum well system we will take the decay and dephasing values non-zero and equal to $\Gamma_1 = 1/66$ ps^{-1} and $\Gamma_2 = 1/6.6$ ps^{-1} as in a previous study in the same quantum well structure [25].

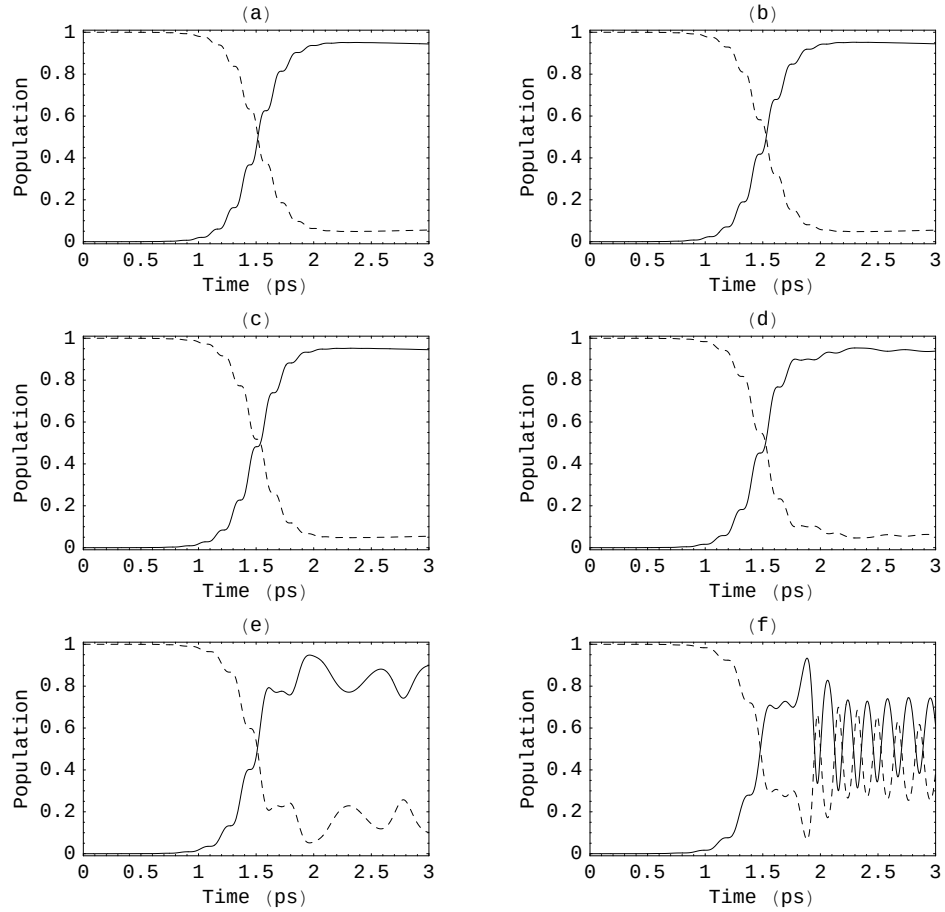

FIGURE 2. The same as in figure 1 but for a hyperbolic secant electromagnetic pulse. In these calculations $\Omega_0 = \sqrt{\alpha^2/4 + 1/t_p^2}$, $\omega = \omega_{10}$, $t_p = 0.25$ ps and $t_0 = 1.5$ ps.

In figure 1 we present the time evolution of the population in the lower subband and the upper subband obtained from numerical solutions of the nonlinear density matrix equations (1) and (2) for a CW electromagnetic field with Rabi frequency $\Omega_0 = \alpha/3$. The field is at exact resonance with the transition frequency ω_{10}. Figures 1(a)-1(f) are for different values of the electron sheet density, in the region $N = 4 \times 10^{10}$ cm^{-2} to $N = 4 \times 10^{11}$ cm^{-2}. In all cases we plot the populations up to $t = T/2$, where the period T is given from formula (8), as $\Omega_0 > \alpha/4$.

We first note that complete population transfer in the upper subband does not occur in this case. This is expected as Γ_1 and Γ_2 are nonzero in this case. However, significant population transfer in the upper subband and high-efficiency intersubband population inversion occurs. In figures 1(a) - 1(d) the internal oscillations are due to existence of non-RWA terms. From, figures 1(a) - 1(e) we note that the increase of the electron sheet density leads to decrease of the period of oscillations and to larger population transfer in the upper subband, as the effects of the relaxation processes become smaller. A comparison with the case that the RWA is applied in the dynamics of the system (not shown here) gives that the the results without the RWA are well described by the RWA results only for figures 1(a) - 1(d). Similar results have been obtained for several other values of Ω_0, in the region that $\Omega_0 > \alpha/4$.

In figures 2 and 3 we present the time evolution of the population in the lower subband and the upper subband obtained from numerical solutions of the nonlinear density matrix equations (1) and (2) for a (transformed-limited)

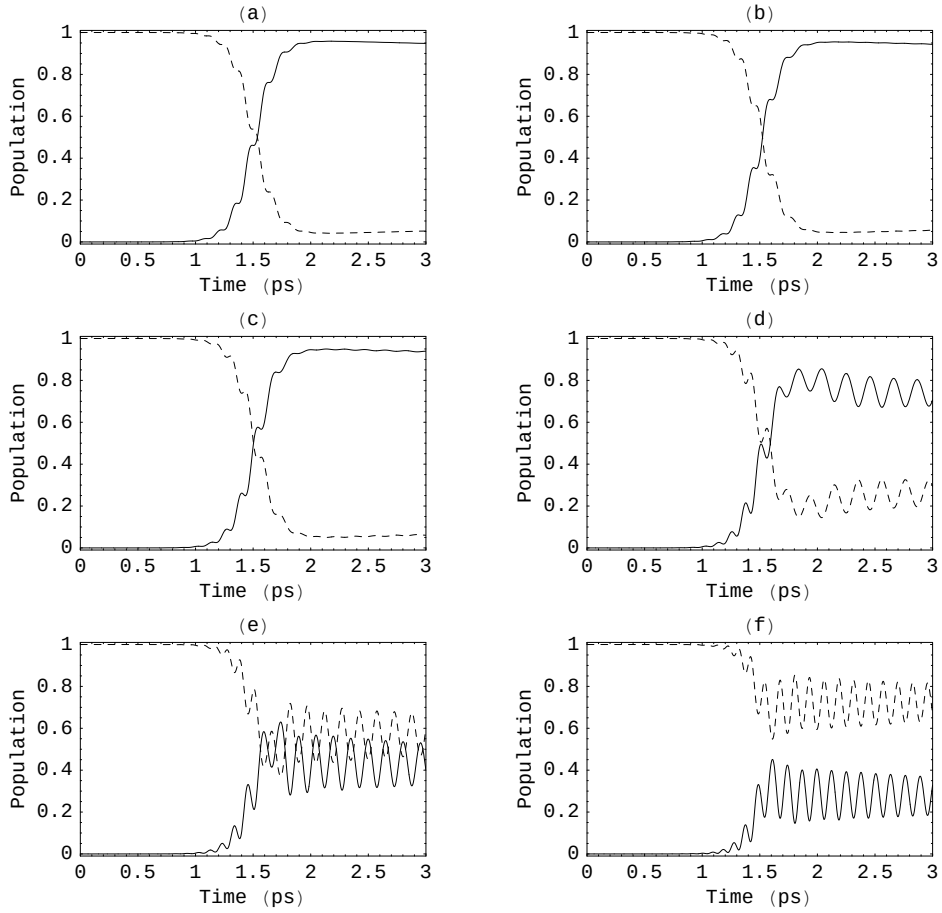

FIGURE 3. The same as in figure 1 but for a chirped hyperbolic secant electromagnetic pulse. In these calculations $\Omega_0 = 1/t_p$, $\omega = \omega_{10}$, $t_p = 0.2$ ps and $t_0 = 1.5$ ps. The time-dependent frequency follows Eq. (11).

hyperbolic secant pulse (figure 2) and a chirped hyperbolic secant pulse (figure 3). From figures 2 and 3 we note that the time evolution of the population in the two subbands is quite similar for the cases that $N = 4 \times 10^{10}$ cm^{-2}, $N = 7 \times 10^{10}$ cm^{-2}, and $N = 1 \times 10^{11}$ cm^{-2}. This can be seen from figures 2(a) - 2(c) and figures 3(a) - 3(c). These results are also described very well by results obtained with the RWA (not shown here). In these cases significant population inversion is created in the system. For larger values of the electron sheet density the time evolution of the system changes and it is not well-described by the RWA results. A comparison of the results of figures 2(d) - 2(f) with figures 3(d) - 3(f) shows us that the (transformed-limited) hyperbolic secant pulse leads to more larger population inversion in the system than the chirped hyperbolic secant pulse, for these values of the electron sheet density.

CONCLUSIONS

In this work we have studied controlled population dynamics in a single semiconductor quantum well, in the two-subband approximation, that is coupled by a strong electromagnetic field. We have used the nonlinear density matrix equations for the description of the system dynamics. We have applied the RWA and have presented analytical solutions of the density matrix equations for three different cases of applied electromagnetic pulses, in the case that no relaxation effects are accounted for. In all the cases the analytical solutions show that complete population transfer in the upper subband occurs, and thus complete population inversion is succeeded. We then assess the validity of the analytical results for obtaining controlled population transfer and high-efficiency population inversion in a realistic GaAs/AlGaAs single quantum well, without applying the RWA, and in the presence of relaxation processes. We show

that in all the cases high-efficiency population inversion is possible if $\alpha \leq \omega_{10}$. In addition, the time-evolution of the complete system is described well by the RWA results if $\alpha \leq \omega_{10}/2$.

ACKNOWLEDGMENTS

We would like to thank Dr. Margarita Tsaousidou for useful discussions and help. We would also like to thank the Research Committee of the University of Patras for financial support under the research project “K. Karatheodoris”.

REFERENCES

1. J. Faist, F. Capasso, C. Sirtori, K.W. West, and L.N. Pfeiffer, *Nature* **390**, 589 (1997).
2. H. Schmidt, K. L. Campman, A. C. Gossard, and A. Imamoglu, *Appl. Phys. Lett.* **70**, 3455 (1997).
3. G. B. Serapiglia, E. Paspalakis, C. Sirtori, K. L. Vodopyanov, and C. C. Phillips, *Phys. Rev. Lett.* **84**, 1019 (2000).
4. C.W. Luo, K. Reimann, M.Woerner, T. Elsaesser, R. Hey, and K. H. Ploog, *Phys. Rev. Lett.* **92**, 047402, (2004).
5. T. Müller, W. Parz, G. Strasser, and K. Unterrainer, *Phys. Rev. B* **70**, 155324 (2004).
6. J. F. Dynes, M. D. Frogley, M. Beck, J. Faist, and C. C. Phillips, *Phys. Rev. Lett.* **94**, 157403 (2005).
7. M. D. Frogley, J. F. Dynes, M. Beck, J. Faist, and C. C. Phillips, *Nature Materials* 5, 175 (2006).
8. S. L. Chuang, M. S. C. Luo, S. Schmitt-Rink, and A. Pinczuk, *Phys. Rev. B* **46**, 1897 (1992).
9. M. Zalużny, *Phys. Rev. B* **47**, 3995 (1993).
10. M. Zalużny, *J. Appl. Phys.* **74**, 4716 (1993).
11. B. Galdrikian and B. Birnir, *Phys. Rev. Lett.* **76**, 3308 (1996).
12. D. E. Nikonov, A. Imamoglu, L. V. Butov and H. Schmidt, *Phys. Rev. Lett.* **79**, 4633 (1997).
13. C.A. Ullrich and G. Vignale, *Phys. Rev. B* **58**, 15756 (1998).
14. D. E. Nikonov, A. Imamoglu, and M.O. Scully, *Phys. Rev. B* **59**, 12212 (1999).
15. A. A. Batista, B. Birnir, and M. S. Sherwin, *Phys. Rev. B* **61**, 15108 (2000).
16. A. A. Batista, P. I. Tamborenea, B. Birnir, M. S. Sherwin and D. S. Citrin, *Phys. Rev. B* **66**, 195325 (2002).
17. J. Z. Li and C. Z. Ning, *Phys. Rev. Lett.* **91**, 097401 (2003).
18. A. Olaya-Castro, M. Korkusinski, P. Hawrylak, and M. Yu. Ivanov, *Phys. Rev. B* **68**, 155305 (2003).
19. P. Haljan, T. Fortier, P. Hawrylak, P. B. Corkum, and M. Yu. Ivanov, *Laser Phys.* **13**, 452 (2003).
20. H. O. Wijewardane and C. A. Ullrich, *Appl. Phys. Lett.* **84**, 3984 (2004).
21. A. A. Batista and D. S. Citrin, *Phys. Rev. Lett.* **92**, 127404 (2004).
22. A. A. Batista, *Phys. Rev. B* **73**, 075305 (2006).
23. E. Paspalakis, M. Tsaousidou and A. F. Terzis, *Phys. Rev. B* **73**, 125344 (2006).
24. E. Paspalakis, M. Tsaousidou and A. F. Terzis, *J. Appl. Phys.* **100**, 044312 (2006).
25. A. A. Batista and D. S. Citrin, *Phys. Rev. B* **74**, 195318 (2004).
26. J. N. Heyman *et al.*, *Phys. Rev. Lett.* **72**, 2183 (1994).
27. M. S. Sherwin *et al.*, *Physica D* **83**, 229 (1995).
28. K. Craig *et al.*, *Phys. Rev. Lett.* **76**, 2382 (1996).
29. T. Müller, W. Parz, G. Strasser, and K. Unterrainer, *Appl. Phys. Lett.* **84**, 64 (2004).
30. T. Müller, W. Parz, G. Strasser, and K. Unterrainer, *Phys. Rev. B* **70**, 155324 (2004).
31. C. D. Simserides and G. P. Triberis, *J. Phys.: Condens. Matter* **5**, 6437 (1993).
32. G.A.M. Hurkx and W. van Haeringen, *J. Phys. C.: Solid State Phys.* **18**, 5617 (1985).
33. F. Stern and S. Das Sarma, *Phys. Rev. B* **30**, 840 (1984).
34. C. D. Simserides, *J. Phys.: Condens. Matter* **11**, 5131 (1999).